Article

Distinct Binding Dynamics, Sites and Interactions of Fullerene and Fullerenols with Amyloid-β Peptides Revealed by Molecular Dynamics Simulations

Zhiwei Liu [1,†], Yu Zou [2,†], Qingwen Zhang [2], Peijie Chen [1], Yu Liu [1] and Zhenyu Qian [1,*]

[1]   Key Laboratory of Exercise and Health Sciences (Ministry of Education), School of Kinesiology, Shanghai University of Sport, 399 Changhai Road, Shanghai 200438, China; 15266070790@163.com (Z.L.); chenpeijie@sus.edu.cn (P.C.); yuliu@sus.edu.cn (Y.L.)

[2]   College of Physical Education and Training, Shanghai University of Sport, 399 Changhai Road, Shanghai 200438, China; zouyu_1993@163.com (Y.Z.); zqw@sus.edu.cn (Q.Z.)

[*]   Correspondence: qianzhenyu@sus.edu.cn

[†]   These authors contributed equally to this work.

check for
updates

Abstract: The pathology Alzheimer's disease (AD) is associated with the self-assembly of amyloid-β (Aβ) peptides into β-sheet enriched fibrillar aggregates. A promising treatment strategy is focused on the inhibition of amyloid fibrillization of Aβ peptide. Fullerene C_{60} is proved to effectively inhibit Aβ fibrillation while the poor water-solubility restricts its use as a biomedicine agent. In this work, we examined the interaction of fullerene C_{60} and water-soluble fullerenol $C_{60}(OH)_6/C_{60}(OH)_{12}$ (C_{60} carrying 6/12 hydroxyl groups) with preformed $Aβ_{40/42}$ protofibrils by multiple molecular dynamics simulations. We found that when binding to the $Aβ_{42}$ protofibril, C_{60}, $C_{60}(OH)_6$ and $C_{60}(OH)_{12}$ exhibit distinct binding dynamics, binding sites and peptide interaction. The increased number of hydroxyl groups C_{60} carries leads to slower binding dynamics and weaker binding strength. Binding free energy analysis demonstrates that the $C_{60}/C_{60}(OH)_6$ molecule primarily binds to the C-terminal residues 31–41, whereas $C_{60}(OH)_{12}$ favors to bind to N-terminal residues 4–14. The hydrophobic interaction plays a critical role in the interplay between Aβ and all the three nanoparticles, and the π-stacking interaction gets weakened as C_{60} carries more hydroxyls. In addition, the $C_{60}(OH)_6$ molecule has high affinity to form hydrogen bonds with protein backbones. The binding behaviors of $C_{60}/C_{60}(OH)_6/C_{60}(OH)_{12}$ to the $Aβ_{40}$ protofibril resemble with those to $Aβ_{42}$. Our work provides a detailed picture of fullerene/fullerenols binding to Aβ protofibril, and is helpful to understand the underlying inhibitory mechanism.

Keywords: amyloid protofibril; fullerene; binding site; inhibitory mechanism; molecular dynamics simulation

1. Introduction

Amyloids are involved in a broad range of neurodegenerative diseases, including Alzheimer's, Huntington's and Parkinson's diseases [1–3]. The major constituents of amyloid plaques are associated with fibrils formed by amyloid-β (Aβ) protein that display a cross-β structure characterized by β-strands perpendicular to and inter-strand hydrogen bonds parallel to the fibril axis [4,5]. The fibrillation occurs through a complex multistep process, involving the formation of soluble oligomers, protofibrils and insoluble mature fibrils [6,7]. Small aggregates (soluble oligomers and protofibrils) in the early stage of aggregation are suggested as primary neurotoxic agents [8–11]. Therefore, a promising strategy to reduce the small toxic oligomer species is to inhibit Aβ peptide aggregation.

The search for effective inhibitors has become an active area of research. An increasing number of experimental and computational studies have reported that Aβ aggregation can be modulated by nanoparticles [12–14], small molecules [15,16], short peptides [17,18], antibodies [19] and metal ions [20]. Their findings provided new clues for the design of inhibitors targeting Aβ formation. In recent years, the fullerenes have gained great attention, not only because of their antioxidant, neuroprotective and antitumor properties [21], but also due to their promising ability of carrying contrast agents, radiopharmaceuticals or drugs [22]. However, the poor solubility of fullerenes in water restricts their potential biomedical applications. One of the common strategies to increase of their solubility is to attach hydroxyl groups to the carbon cage, leading to the formation of hydroxylated fullerene (i.e., fullerenol, $C_{60}(OH)_n$). Fullerenols have high solubility and ability to cross the blood brain barriers [23]. Fullerene derivatives are reported to have remarkable anti-amyloid properties for Alzheimer's disease and other neurodegenerative diseases [24–28].

Computational studies have investigated the molecular mechanism of fullerenes/fullerenols binding and binding-induced protein remodeling using docking method and molecular dynamics (MD) simulations [29–33]. For example, Li et al. examined the binding affinity of fullerenes in different sizes and found that C_{60} destroys pentameric $Aβ_{17–42}$ fibril structure to a greater extent with respect to other fullerenes [29]. They also found that $C_{60}(OH)_{16}$ is inclined to bind at the central hydrophobic and the hydrophobic C-terminal region of monomer $Aβ_{40}$ to prevent amyloid fibrillization [30]. Wei et al. identified three primary binding sites of 1,2-(dimethoxymethano) fullerene (DMF) to $Aβ_{1–42}$ protofibril: the central hydrophobic residues 17–21, the residues 27–31 in turn region and the C-terminal residues 31–41 [31]. They also demonstrated that the fullerene nanoparticles – C_{60} and C_{180} exhibit stronger inhibition on $Aβ_{16–22}$ β-sheet formation [33]. Ding et al. found that different extent of hydroxylation would significantly influence $C_{60}(OH)_n$–protein interactions [32]. These results reveal the binding modes and inhibitory/disruptive mechanisms of fullerenes/fullerenols, which greatly enhances our understanding of fullerenes/fullerenols-protein interactions at atomic level.

Our previous study examined the influence of DMF on $Aβ_{42}$ dimerization by replica-exchange MD simulations [34]. However, the interactions between Aβ protofibril and fullerenes with different degree of hydroxylation remain elusive. Previous computational study showed that stable Aβ trimer with well-preserved parallel β-strands could act as the smallest seed for Aβ polymerization on self-assembled monolayers [35]. Following the work by Zheng and Wei [35,36], we chose a trimer as Aβ protofibril model in our MD simulations. Here, we investigated the interaction of a $C_{60}/C_{60}(OH)_6/C_{60}(OH)_{12}$ molecule with $Aβ_{42/40}$ protofibrillar trimer and the resulting protein structural alterations by performing multiple MD simulations. We found that the increased hydroxylation extent of C_{60} leads to slower binding dynamics and weaker binding strength. Binding sites and free energy analyses demonstrate that the $C_{60}/C_{60}(OH)_6$ molecule primarily binds to the C-terminal hydrophobic region, whereas $C_{60}(OH)_{12}$ favors to bind to N-terminal residues 4–14. Our simulations revealed the dominant role of hydrophobic interaction in Aβ−nanoparticle interplay. Moreover, the water-soluble $C_{60}(OH)_6$ molecule has high affinity to form hydrogen bonds with protein backbones, which makes it a more efficient inhibitor than C_{60} and $C_{60}(OH)_{12}$.

2. Results and Discussion

We performed MD simulations to study the binding behavior of $C_{60}/C_{60}(OH)_6/ C_{60}(OH)_{12}$ to $Aβ_{42}$ protofibrillar trimer ($Aβ_{42}$-trimer for short) and $Aβ_{40}$ protofibrillar trimer ($Aβ_{40}$-trimer for short), respectively. The systems are labeled as $Aβ_{42}$-trimer-C_{60}, $Aβ_{42}$-trimer-$C_{60}(OH)_6$, $Aβ_{42}$-trimer-$C_{60}(OH)_{12}$, $Aβ_{40}$-trimer-C_{60}, $Aβ_{40}$-trimer-$C_{60}(OH)_6$ and $Aβ_{40}$-trimer-$C_{60}(OH)_{12}$. The molecular structures of $Aβ_{42}$-trimer, $Aβ_{40}$-trimer and $C_{60}/C_{60}(OH)_6/C_{60}(OH)_{12}$ are shown in Figure 1. The initial state of $Aβ_{42}$-trimer-C_{60} system is also displayed, and the other systems are constructed similarly. More details are given in Model and Methods section.
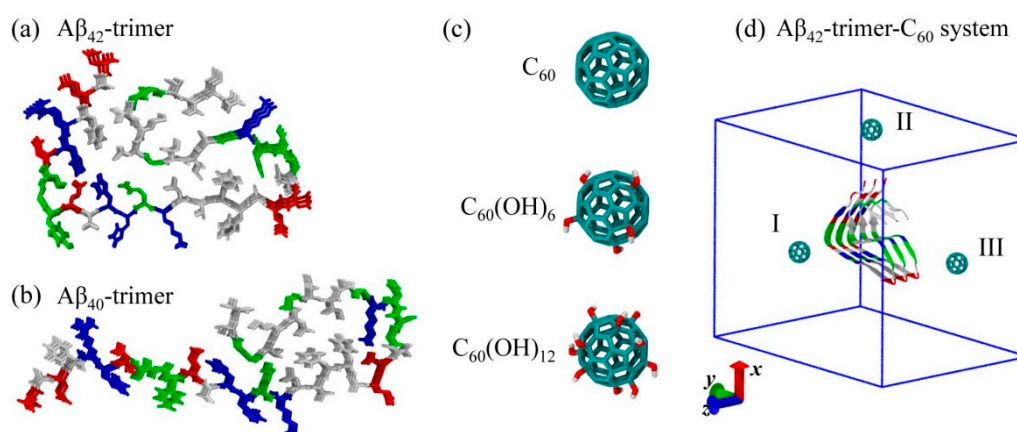
Figure 1. Molecular structures and simulation system setup. (**a**–**c**) The structures of Aβ$_{42}$-trimer, Aβ$_{40}$-trimer and C$_{60}$/C$_{60}$(OH)$_6$/C$_{60}$(OH)$_{12}$. (**d**) The initial conformation of the Aβ$_{42}$-trimer-C$_{60}$ system with the C$_{60}$ molecule placed at three different positions (I-III). Color codes: positively charged residues (blue), negatively charged residues (red), hydrophobic residues (white) and polar residues (green) in Aβ peptides; carbon atoms (cyan), oxygen atoms (red) and hydrogen atoms (white) in fullerene/fullerenol. For clarity, water molecules in the simulation box are not displayed; box vectors are shown, and *z*-axis is the fibrillar elongation direction.

2.1. Dynamics of the Fullerene/Fullerenol Molecule Binding to Aβ$_{42}$-Trimer

To investigate the binding process of the fullerene/fullerenol molecule to Aβ$_{42}$-trimer, we first monitored the time evolution of their minimum distance d_{min} (Figure 2a–c). As for the Aβ$_{42}$-trimer-C$_{60}$ system, the C$_{60}$ molecule was initially placed 2 nm away from the Aβ$_{42}$-trimer. Once the MD simulations were initiated, d_{min} started to decrease or increase, depending on the initial velocity distributions. The minimum distances in Run 1, 2 and 4 were observed to decline to ~0.30 nm within the first 3 ns, while those in Run 3, 5 and 6 took ~10 ns to reach ~0.30 nm. Such fast and slow binding processes were also observed in Aβ$_{42}$-trimer-C$_{60}$(OH)$_6$ and Aβ$_{42}$-trimer-C$_{60}$(OH)$_{12}$ systems. Similar fast and slow processes were reported in a previous MD study of DMF binding to Aβ fibril [31]. Moreover, we found that the slow binding processes may last tens of nanoseconds for C$_{60}$(OH)$_6$ and C$_{60}$(OH)$_{12}$, much longer than that for C$_{60}$. It takes over 25 ns for two MD runs of Aβ-C$_{60}$(OH)$_6$ system (Runs 3, 6) to reach a minimum distance of ~0.30 nm, and the situation was the same in Aβ-C$_{60}$(OH)$_{12}$ system (Runs 3, 4). Specially, in Run 3 of Aβ$_{42}$-trimer-C$_{60}$(OH)$_{12}$ system, d_{min} increased sharply at 49.8 and 83.6 ns, and declined to ~0.30 nm in the next twenty nanoseconds. These indicate that the binding process of the C$_{60}$(OH)$_6$/C$_{60}$(OH)$_{12}$ molecule to Aβ$_{42}$-trimer is slower than that of C$_{60}$.

To further examine the binding status of the fullerene/fullerenol molecule after the initial adsorption to Aβ$_{42}$-trimer, we monitored the time evolution of the number of contacts between individual residue and the nanoparticle in a representative MD run for each simulated system in Figure 2d–f. The C$_{60}$ molecule was observed to stay at a relatively fixed location during the remaining simulation time once stable contacts are formed. The C$_{60}$(OH)$_6$ molecule also had a relatively fixed binding site, while it can shift to other location transiently. As for the C$_{60}$(OH)$_{12}$ molecule, its binding location kept changing when simulation time increased, corresponding to a slow move on the protein surface. C$_{60}$(OH)$_{12}$ also contacted with more residues at the same time, which indicated a lower specificity of binding sites. These results reflect that with the hydroxylation extent of C$_{60}$ increased, the binding strength between Aβ$_{42}$-trimer and the nanoparticle molecule gets weaker.
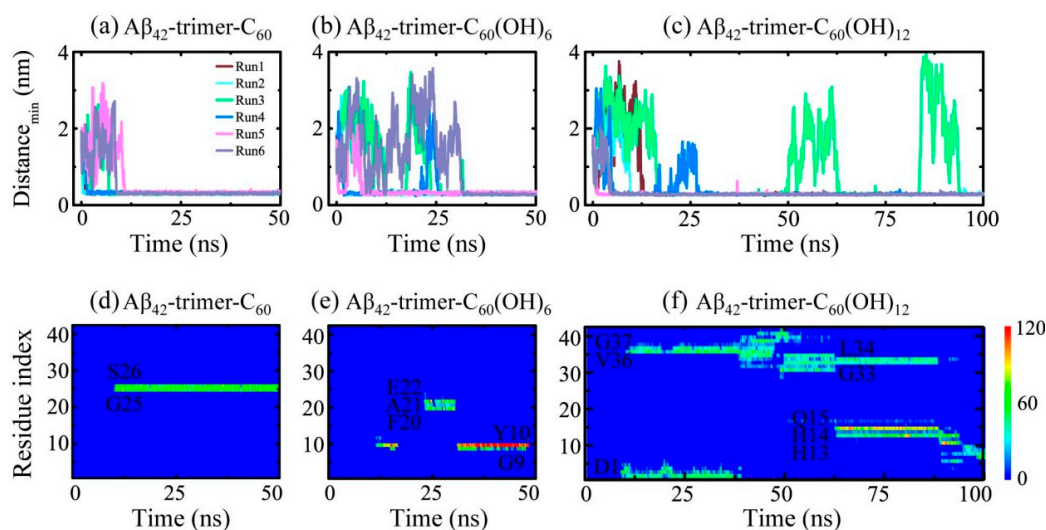
Figure 2. Dynamics of the fullerene/fullerenol molecule binding to Aβ$_{42}$-trimer. (**a–c**) Time evolution of the minimum distance between Aβ$_{42}$-trimer and fullerene/fullerenol. Six independent molecular dynamics (MD) runs are denoted in different colors. (**d–f**) Time evolution of the number of contacts between individual residue of Aβ$_{42}$-trimer and fullerene/fullerenol in a representative MD run for each simulated system.

In order to quantify the binding strength, we calculated in Table 1 the binding free energy and its different components between Aβ$_{42}$-trimer and the fullerene/fullerenol molecule using the MM/PBSA (molecular mechanics/linear Poisson−Boltzmann surface area) method. The binding energy was calculated over all six MD runs for each simulated system using the last 20 ns data of each MD trajectory. The binding energy components show that the van der Waals interaction (ΔE_{vdW}) has a dominant contribution to the total binding energy (ΔG_{bind}). It is shown that ΔE_{vdW} is -24.02 ± 0.74 kcal/mol in the Aβ-C$_{60}$ system, -24.02 ± 0.74 kcal/mol in the Aβ-C$_{60}$(OH)$_6$ system and -18.20 ± 1.02 kcal/mol in the Aβ-C$_{60}$(OH)$_{12}$ system. Interestingly, although C$_{60}$(OH)$_6$ carries six more hydroxyl groups than C$_{60}$, their ΔE_{vdW} is quite similar, and that of C$_{60}$(OH)$_{12}$ became ~6 kcal/mol larger. This reveals that the increment of ΔE_{vdW} is not in proportion to the hydroxylation level of C$_{60}$ surface. Due to the additional partial charges that hydroxyls bring, the electrostatic interaction (ΔE_{elec}) is strengthened as the hydroxyl number increases. The nonpolar solvation component $\Delta G_{nonpolar}$ contributes little to the free energy change. The enhanced hydrophilicity with the addition of hydroxyls results in a positive value of ΔG_{solv} (solvation effect), indicating that water is favorable for fullerenols and solvation effect goes against the binding of fullerenol to Aβ. Our results are consistent with a previous study on fullerenol C$_{60}$(OH)$_{16}$ interacting with Aβ$_{40}$ [30]. They found that the electrostatics contribution is much increased in fullerenol with respect to that in fullerenes, yet hydroxyl groups contribute a positive amount to the binding free energy. Overall, our free energy calculation demonstrates that the total binding free energy rises with more hydroxyl groups attached to C$_{60}$. This gives the explanation that higher hydroxylation level leads to slower binding dynamics and weaker binding strength.

Table 1. Different components of binding free energy (in kcal/mol) between Aβ$_{42}$-trimer and the fullerene/fullerenol molecule.

Systems	ΔE_{vdw}	ΔE_{elec}	ΔE_{MM}	ΔG_{polar}	$\Delta G_{nonpolar}$	ΔG_{solv}	ΔG_{bind}
Aβ$_{42}$-trimer-C$_{60}$	−24.44 ± 0.69	0	−24.44 ± 0.69	0	−3.92 ± 0.16	−3.92 ± 0.16	−28.36 ± 0.71
Aβ$_{42}$-trimer-C$_{60}$(OH)$_6$	−24.02 ± 0.74	−5.16 ± 0.69	−29.18 ± 0.25	15.27 ± 1.68	−3.61 ± 0.16	11.66 ± 1.69	−17.52 ± 1.71
Aβ$_{42}$-trimer-C$_{60}$(OH)$_{12}$	−18.20 ± 1.02	−14.60 ± 1.45	−32.80 ± 1.77	27.06 ± 2.52	−3.30 ± 0.17	23.77 ± 2.53	−9.03 ± 3.09

2.2. Binding Sites of The Fullerene/Fullerenol Molecule to Aβ42-Trimer

Identifying the binding sites of the C_{60}/$C_{60}(OH)_6$/$C_{60}(OH)_{12}$ molecule to Aβ42-trimer is the first step to understand the underlying inhibition mechanism. To this aim, we calculated the residue-based binding free energy of the nanoparticles to Aβ42-trimer in Figure 3a–c using last 20 ns data of the simulations. As shown, C_{60} has the lowest binding energy with aromatic residue F4, and hydrophobic residues V39 and A2, as well as G25 located in the turn region; $C_{60}(OH)_6$ has the lowest binding energy with aromatic Y10 and F4, negatively charged E11, and hydrophobic L34, L17 and V39; $C_{60}(OH)_{12}$ has the lowest binding energy with hydrophobic L34, negatively charged E22 and aromatic F4. This indicates the critical roles of aromatic stacking and hydrophobic interactions in the interplay between Aβ and all the three nanoparticles. As for fullerenols $C_{60}(OH)_6$ and $C_{60}(OH)_{12}$, their hydrogen bonding interaction with negatively charged residues of Aβ is also important.
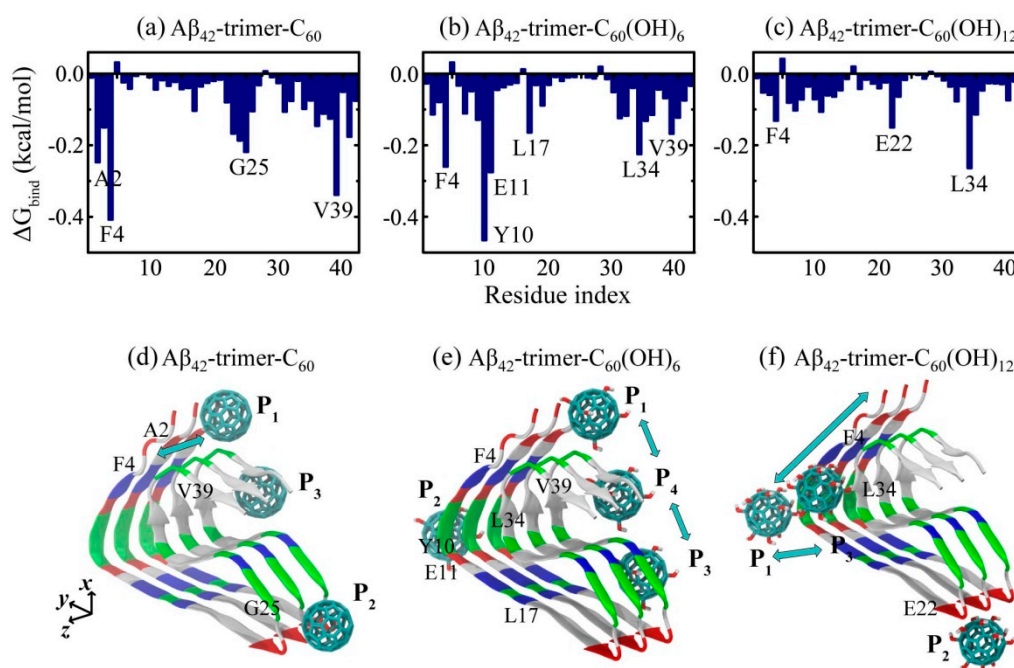
Figure 3. Analysis of binding sites of the fullerene/fullerenol molecule to Aβ42-trimer. (**a–c**) Residue-based binding free energy. The binding energy was calculated over all six MD runs for each simulated system using the last 20 ns data of each MD trajectory. (**d–f**) Schematic diagrams for binding sites of the fullerene/fullerenol molecule to Aβ42-trimer. The positions where the fullerene/fullerenol molecule has high binding affinity are named with P_1, P_2, etc., from N-termini to C-termini, and *z*-axis is the fibrillar elongation direction. The color code is consistent with that in Figure 1.

According to the residue-based binding free energy, we found that C_{60} preferentially interacts with Aβ42-trimer at three different sites: 2AEF4, 23DVG25 and C-terminal residues 31–41. Through the binding energy analysis at each site (Table 2), we found that C-terminal residues 31–41 and 2AEF4 have the lowest binding energy, indicating these two regions are the most favorable binding sites for C_{60}. This finding is in agreement with the binding sites (aromatic residues F4 and C-terminal hydrophobic residues 31–40) identified in DMF interacting with Aβ dimer [34]. The C-terminal hydrophobic region of residues 31–41 was also reported to be the dominant binding site in DMF interacting with Aβ fibrillar hexamer [31]. As for $C_{60}(OH)_6$, it prefers to bind to Aβ42-trimer at four sites: 2AEF4, 9GYE11, 17LVF19 and C-terminal residues 31–41, among which C-terminal residues 31–41 and 9GYE11 have the lowest binding energy. As for $C_{60}(OH)_{12}$, it has three preferential sites: N-terminal residues 4–14, 22ED23 and 34LM35, among which N-terminal residues 4–14 are the most favorable. The hydrophobic clusters A2-F4-L34-V36, L17-F19-I31 and A30-I32-M35-V40 play critical roles in the structural stability

of Aβ_{42} fibril [5]. The strong binding of C$_{60}$/C$_{60}$(OH)$_6$ to these clusters is expected to interfere with the hydrophobic packing of Aβ side chains, and as a result goes against further fibrillization.

Table 2. Free energy (in kcal/mol) of different binding sites for the fullerene/fullerenol molecule to Aβ_{42}-trimer.

| System	Aβ_{42}-trimer-C$_{60}$			Aβ_{42}-trimer-C$_{60}$(OH)$_6$				Aβ_{42}-trimer-C$_{60}$(OH)$_{12}$		
Binding site	2–4	23–25	31–41	2–4	9–11	17–19	31–41	4–14	22–23	34–35
ΔG_{bind}	−0.80	−0.57	−1.32	−0.45	−0.87	−0.28	−1.23	−0.73	−0.21	−0.38
Deviation	0.09	0.02	0.01	0.06	0.03	0.04	0.05	0.07	0.04	0.05

To exhibit the relation between binding dynamics and binding sites clearly, we presented the schematic diagrams for binding sites of C$_{60}$/C$_{60}$(OH)$_6$/C$_{60}$(OH)$_{12}$ to Aβ_{42}-trimer. The positions where the fullerene/fullerenol molecule has high binding affinity are named with P$_1$, P$_2$, etc., from *N*-termini to *C*-termini. As shown in Figure 3d, there are three positions P$_1$, P$_2$ and P$_3$ at which C$_{60}$ prefers to stay when binding to Aβ_{42}-trimer, mainly corresponding to the binding sties 2AEF4, 23DVG25 and C-terminal residues 31–41, respectively. Note that C$_{60}$ staying at P$_1$ can interact with the region 2AEF4 and the C-terminal residues 31–41 at the same time. Trajectory tracing shows that C$_{60}$ binds mostly at P$_1$ and P$_3$ with a respective probability of 22.7% and 29.8%, in agreement with the free energy calculation, and the location of C$_{60}$ is relatively fixed. Moreover, the C$_{60}$ molecule is able to wander on the surface groove along *z*-axis of Aβ_{42}-trimer at P$_1$ position. These preferential positions are near two hydrophobic clusters A2-F4-L34-V36 and A30-I32-M35-V40, indicating that the binding of C$_{60}$ to Aβ_{42}-trimer is dominantly driven by the hydrophobic interaction. The importance of hydrophobic interaction was reported in other studies on the binding processes of fullerene and other small molecules to Aβ [29,37,38]. With respect to P$_1$ and P$_3$, C$_{60}$ has a relatively lower binding affinity to P$_2$. This binding site is facilitated by the groove of a proper size in the 23DVGS26 region, where the side chains of D23 and S26 are in the outer side of Aβ_{42}-trimer and G25 has no side chain. Similar concave-induced binding sites were observed in the study of fullerenes with Aβ and other proteins [31,39,40].

As for C$_{60}$(OH)$_6$, it has four preferential binding positions P$_1$, P$_2$, P$_3$ and P$_4$ (Figure 3e), mainly corresponding to the binding sties 2AEF4, 9GYE11, 17LVF19 and C-terminal residues 31–41, respectively. Interestingly, the C$_{60}$(OH)$_6$ molecule is able to slip on the elongation surface (perpendicular to *z*-axis), wandering between P$_1$ and P$_4$ or between P$_3$ and P$_4$ with a low probability. The P$_3$ position is adjacent to another hydrophobic cluster L17-F19-I31 of Aβ_{42}-trimer. Besides, C$_{60}$(OH)$_6$ has high binding affinity to 9GYE11 (P$_2$), facilitated by the hydrogen bonds (H-bonds) formed in between. As for C$_{60}$(OH)$_{12}$, it prefers to bind to three positions P$_1$, P$_2$ and P$_3$ (Figure 3f), corresponding to the binding sties N-terminal residues 4–14, 22ED23 and 34LM35, respectively. Different from the binding behaviors of C$_{60}$ and C$_{60}$(OH)$_6$, C$_{60}$(OH)$_{12}$ is more likely to stay at the hydrophilic parts of protein surface. It is able to move between positions P$_1$ and P$_3$, or slip along the N-terminal β-strand, forming H-bonds with main chain or side chain of amino acids. The C$_{60}$(OH)$_{12}$ molecule may also contact with 22ED23 region. As the side chains of E22 and D23 are oriented to water solution, C$_{60}$(OH)$_{12}$ is inclined to form H-bonds with them. Considering the important roles of C-terminal hydrophobic residues in Aβ aggregation and toxicity [41–43], it is conceivable that the binding of C$_{60}$ and C$_{60}$(OH)$_6$ molecules to the C-terminal region can prevent Aβ fibrillization. In addition, the C$_{60}$(OH)$_6$ molecule has higher affinity to bind to elongation surfaces than C$_{60}$ and C$_{60}$(OH)$_{12}$, which makes C$_{60}$(OH)$_6$ a more effective inhibitor. As previous computational and experimental studies suggested that binding at fibril ends goes against fibrillar elongation [44–46], this binding would block the backbone amide sites for fibril growth and as a result, slows down or inhibits the elongation process. It is noted that the bindings of nanoparticles to protofibril and mature fibril are supposed to be distinct, because the relative area of the exposed ends compared to the entire fibril surface will be greatly decreased in mature fibrils.

2.3. Structural Influence of The Fullerene/Fullerenol Molecule on $A\beta_{42}$-Trimer

In order to detect the influence of fullerene/fullerenol binding on the $A\beta_{42}$-trimer structure, we first examined the secondary structural difference relative to the isolated $A\beta_{42}$-trimer. The β-sheet contents of $A\beta_{42}$-trimer, $A\beta_{42}$-trimer-C_{60}, $A\beta_{42}$-trimer-$C_{60}(OH)_6$ and $A\beta_{42}$-trimer-$C_{60}(OH)_{12}$ systems are 80.5%, 83.3%, 81.1% and 80.4%, respectively, showing little difference. Then, we calculated the average Cα-root-mean-square deviation (Cα-RMSD) with respect to the initial coordinates of $A\beta_{42}$ protofibrillar trimer using the last 20 ns data of each MD trajectory. As shown in Figure 4a, the values of Cα-RMSD in the absence and presence of the $C_{60}(OH)_{12}$ molecule are 0.27 ± 0.03 nm and 0.27 ± 0.01 nm, showing no statistically significant difference. In the presence of $C_{60}/C_{60}(OH)_6$, $A\beta_{42}$-trimer has an increased Cα-RMSD of 0.32 ± 0.02 / 0.34 ± 0.05 nm, while the values are still within the error of estimate with respect to that of isolated Aβ. These indicate that the $C_{60}/C_{60}(OH)_6/C_{60}(OH)_{12}$ molecule has a negligible influence on the structural stability of $A\beta_{42}$-trimer.

Figure 4b,c display the time evolution of Cα-RMSD of the MD trajectory contributing most to the total Cα-RMSD in $A\beta_{42}$-trimer-C_{60} and $A\beta_{42}$-trimer-$C_{60}(OH)_6$ systems, respectively. With C_{60}, the Cα-RMSD value of $A\beta_{42}$-trimer keeps rising in the first 20 ns and finally fluctuates at around 0.55 nm. During this process, the C_{60} molecule is observed to contact abundantly with side chains of V39 and I41, and lead to twisted C-termini. In the $A\beta_{42}$-trimer-$C_{60}(OH)_6$ system, the Cα-RMSD value of $A\beta_{42}$-trimer keeps at ~0.30 nm until t = 40.8 ns. After that, it rises sharply and increases to >1.0 nm. When Cα-RMSD begins its quick rise, the $C_{60}(OH)_6$ molecule is observed to bind at the C-terminal residues 31–41, and the hydrophobic cluster A2-F4-L34-V36 starts to collapse. Then, the sidechains of A2 and F4 dissociate with those of L34 and V36 one by one, and finally the N-termini and C-termini get separated far away. Note that it is the only MD trajectory among all the simulations we performed in this study that N- and C-termini dissociation is observed. It needs further studying to connect this dissociation with Aβ-$C_{60}(OH)_6$ interaction explicitly.
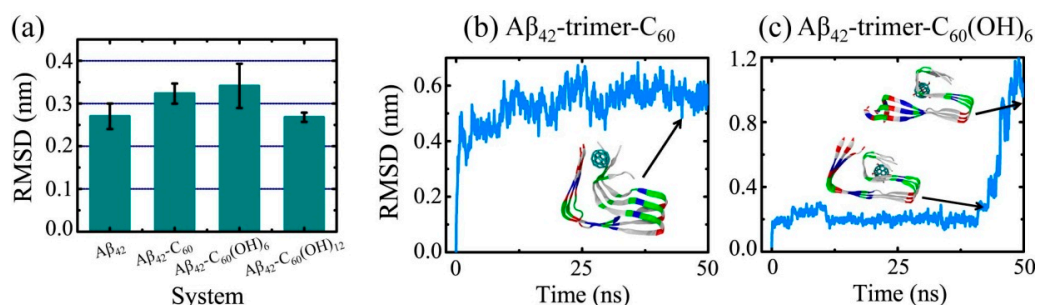
**Figure 4.** Influence of fullerene/fullerenol molecules on the $A\beta_{42}$-trimer structure. (**a**) The average Cα-root-mean-square deviation (Cα-RMSD) relative to the initial coordinates of $A\beta_{42}$ protofibrillar trimer. The values for Aβ-fullerene/fullerenol systems were calculated over all six MD runs for each simulated system using the last 20 ns data of each MD trajectory, and those for isolated $A\beta_{42}$-trimer systems were averaged over the last 50 ns data of two independent 200-ns MD runs. (**b,c**) Time evolution of Cα-RMSD of the MD trajectory that contributes most to the total Cα-RMSD in $A\beta_{42}$-trimer-C_{60} and $A\beta_{42}$-trimer-$C_{60}(OH)_6$ systems, respectively. The color code of the inset snapshots is consistent with that in Figure 1.

The detailed interactions between $A\beta_{42}$-trimer and the fullerene/fullerenol molecule were also investigated. As a previous study suggested that the salt bridges between H6, E11 and H13 stabilize the kink in the N-terminal part of the β-sheets around Y10 [5], we examined the interplay of H6-E11-H13 and found that the interaction pairs stably stay together in all simulated systems except for one MD trajectory of $A\beta_{42}$-trimer-$C_{60}(OH)_6$ system. This trajectory corresponds to the MD run shown in Figure 4c, and its snapshot of the final state is presented in Figure 5a. Even if the *N*- and *C*-termini are

dissociated, the interaction pairs of H6, E11 and H13 mostly stay together, and the interactions of side chains are weakened by excluding those of H6-3 (H6 in Chain 3) and E13-1 (E13 in Chain 1).

In Figure 5b,c, we calculated the number of H-bonds formed between individual residue and fullerenols. It shows that $C_{60}(OH)_6$ favors H-bonding with main chains of $A\beta_{42}$-trimer, and forms H-bonds mostly with residues I32 and D1. The $C_{60}(OH)_{12}$ molecule forms almost the same amount of H-bonds with main chains and side chains, and it preferentially forms H-bonds with residues E11, H13, Q15, D23, E22 and V36. Previous Thioflavin T (ThT) fluorescence and atomic force microscopy experiments showed that fullerenol $C_{60}(OH)_{16}$ can prevent $A\beta_{40}$ fbrillization [30]. The recent study using ThT assay and transmission electron microscope demonstrated that fullerenemalonate can inhibit $A\beta_{42}$ aggregation [47]. Their computational results showed that the inhibition is attributed to the hydrogen bonding of the fullerenemalonate carboxylate groups with $A\beta$. Here, the formation of H-bonds between main chains and fullerenols is supposed to block the backbone amide sites for further addition of peptides in β-sheet structure, which goes against the oligomerization or fibrillization of $A\beta$. The higher affinity of $C_{60}(OH)_6$ bonding with main chains of $A\beta$ peptides makes $C_{60}(OH)_6$ a more efficient inhibitor than $C_{60}(OH)_{12}$.
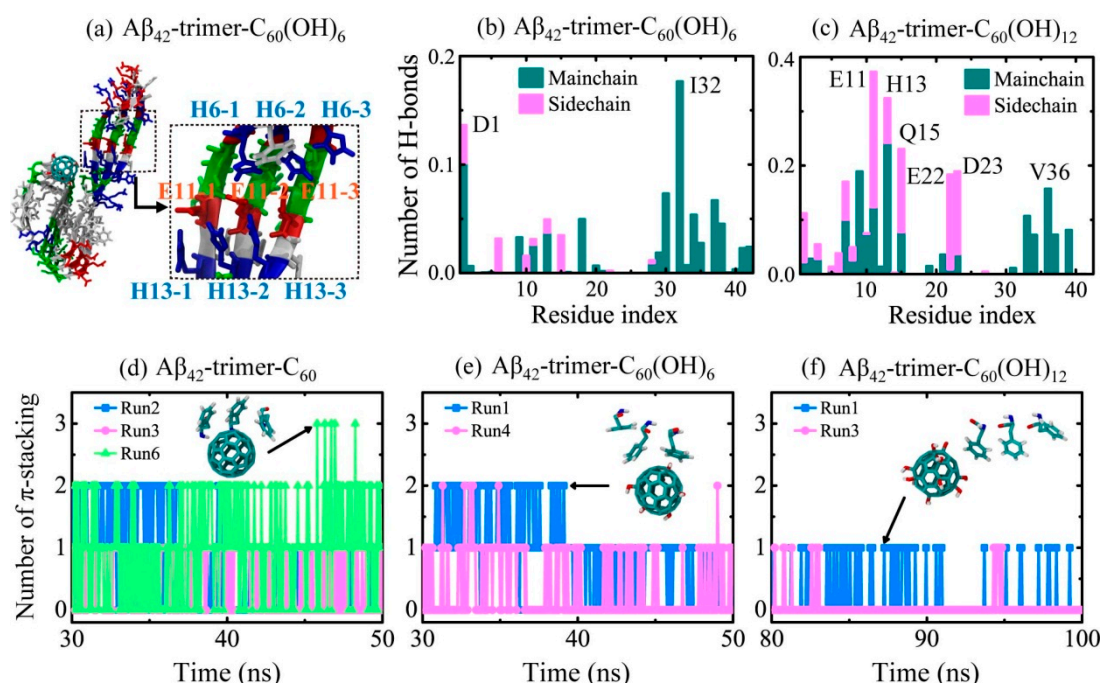
Figure 5. Details of interactions between $A\beta_{42}$-trimer and the fullerene/fullerenol molecule. (**a**) Disturbance to the interplay of H6-E11-H13 observed in a trajectory of $A\beta_{42}$-trimer-$C_{60}(OH)_6$ system. (**b,c**) Number of H-bonds formed between $A\beta_{42}$-trimer and fullerenols. (**d–f**) Number of π-stacking structures between $A\beta_{42}$-trimer and fullerene/fullerenol. The geometrical criterions of H-bonding and π-stacking formations are defined in Model and Methods section.

The π-stacking interaction is important in the self-assembly of amyloid fibrils, with parallel, T-shaped and herringbone (~50°) orientations suggested for aromatic rings in proteins [48]. The binding energy analysis reveals the important role of F4 in the interaction between $A\beta_{42}$-trimer and the fullerene/fullerenol molecule. To examine the aromatic stacking interaction between F4 and $C_{60}/C_{60}(OH)_6/C_{60}(OH)_{12}$, we calculated the number of π-stacking structures between $A\beta42$-trimer and fullerene/fullerenol during the last 20 ns in Figure 5d–f. For the $A\beta_{42}$-trimer-C_{60} system, π-stacking structures were observed in three MD trajectories. Run 6 had the largest number of π-stacking structures, and the maximum number was three. This means that the C_{60} molecule is able to have π-stacking interaction with all the aromatic rings of F4 in $A\beta_{42}$-trimer at the same time. The inset snapshot displays the corresponding structure, and the aromatic rings of F4 are oriented in parallel or herringbone

alignment relative to the C_{60} surface. As for $C_{60}(OH)_6$, it forms less π-stacking structures with $A\beta_{42}$-trimer, and the maximum number of π-stacking decreases to two. For the $A\beta_{42}$-trimer-$C_{60}(OH)_{12}$ system, π-stacking structures are observed in two trajectories and the total number of π-stacking structures is the least. Only one aromatic ring of F4 can have π-stacking interaction with the $C_{60}(OH)_{12}$ molecule at one moment, and the ring is mostly oriented in herringbone alignment relative to the carbon surface of $C_{60}(OH)_{12}$. These results indicate that the more hydroxylated C_{60} is, the fewer and weaker π-stacking interactions with $A\beta_{42}$-trimer the nanoparticle has.

2.4. Dynamics, Sites and Interactions of The Fullerene/Fullerenol Molecule Binding to $A\beta_{40}$-Trimer

We also carried out multiple MD simulations to examine the binding dynamics, binding sites and interactions of the $C_{60}/C_{60}(OH)_6/C_{60}(OH)_{12}$ molecule with $A\beta_{40}$-trimer. Although the structure of $A\beta_{40}$-trimer is different from that of $A\beta_{42}$-trimer (see Figure 1), the binding behavior of nanoparticles to $A\beta_{40}$-trimer was found to display a remarkable resemblance with that to $A\beta_{42}$-trimer. As shown in Figure 6, with the hydroxylation extent increased, the C_{60} molecule displays slower binding dynamics, corresponding to weakened binding strength. The binding free energy analysis shows that the favorable residues of $A\beta_{40}$-trimer with which the nanoparticle tend to interact are a little different from those of $A\beta_{42}$-trimer. Still, these residues are mostly hydrophobic or aromatic, indicating the critical roles of hydrophobic and aromatic interactions in Aβ-nanoparticle interactions. Moreover, the preferential binding regions of the nanoparticles interplaying with $A\beta_{40}$-trimer resemble with those of the nanoparticles binding to $A\beta_{42}$-trimer. We also examined the stability of the D23-K28 salt bridge, which is important for the structural stability of $A\beta_{40}$ [4]. The salt bridge would be interfered by the nanoparticle binding, whereas the connection between the salt bridge disruption and the hydroxylation extent of C_{60} is not explicit.
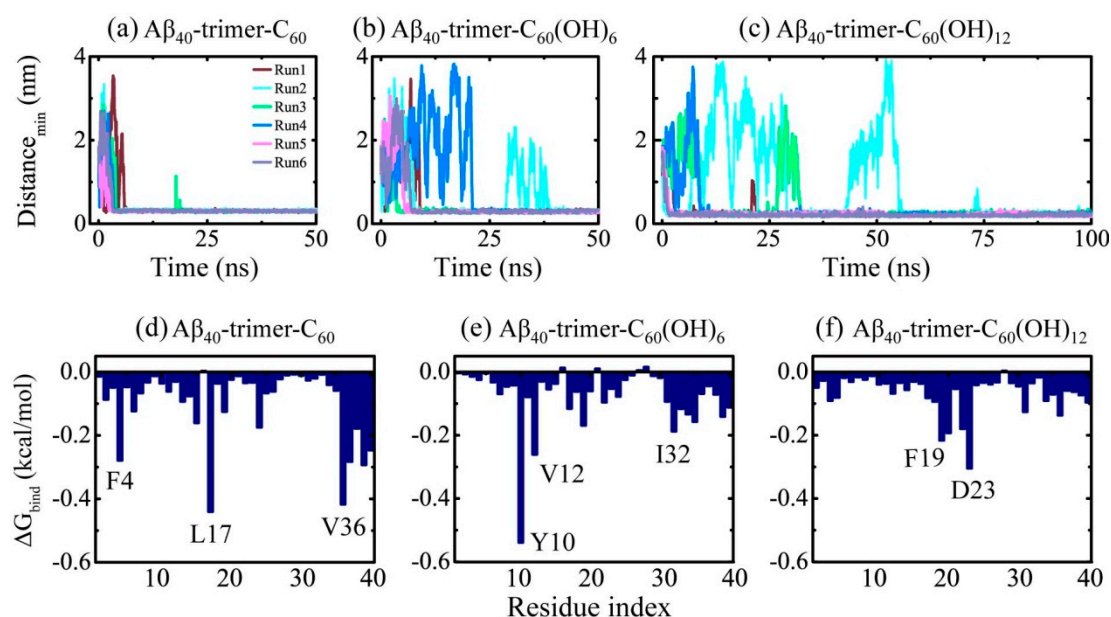
Figure 6. (**a–c**) Time evolution of the minimum distance between $A\beta_{40}$-trimer and fullerene/fullerenol. Six independent MD runs are denoted in different colors. (**d–f**) Residue-based binding free energy. The binding energy was calculated over all six MD runs for each simulated system using the last 20 ns data of each MD trajectory.

3. Materials and Methods

3.1. $A\beta_{40/42}$ Protofibrillar Trimer and $C_{60}/C_{60}(OH)_6/C_{60}(OH)_{12}$ Molecules

The Aβ peptide (39–43-amino acid) is derived from the amyloid precursor protein (APP) through proteolytic cleavage by β- and γ-secretase, and the most abundant Aβ are $A\beta_{42}$ (sequence:

DAEFRHDSGY^{10}EVHHQKLVFF^{20}AEDVGSNKGA^{30}IIGLMVGGVV^{40}IA) and Aβ_{40}. The initial coordinate of the Aβ_{42} protofibrillar trimer was taken from the Aβ_{42} fibril structure [5] (PDB ID: 5OQV) determined by cryo–electron microscopy (cryo-EM). The coordinate of the Aβ_{40} protofibrillar trimer was taken from the Aβ_{40} fibril structure [4] (PDB ID: 2M4J) obtained from solid-state nuclear magnetic resonance (NMR) spectroscopic data. The protonation of the peptide was adjusted to the neutral pH. The *N*- and *C*-termini were respectively capped by NH$_3^+$ and COO$^-$ in accordance with experiments.

The structure of C$_{60}$/C$_{60}$(OH)$_6$/C$_{60}$(OH)$_{12}$ molecules used in this study is displayed in Figure 1. The force field parameters were taken from a previous MD study on the interaction of Aβ and hydroxylated carbon nanotube [49]. To simplify the modeling, the hydroxyl groups in C$_{60}$(OH)$_6$/C$_{60}$(OH)$_{12}$ molecules are distributed uniformly on the C$_{60}$ surface.

The Aβ_{42}-trimer-C$_{60}$ simulation system consists of an Aβ_{42} protofibrillar trimer and a C$_{60}$ molecule placed 2.0 nm (minimum distance) away from Aβ, as shown in Figure 1. To remove the bias of the initial position of C$_{60}$ on the binding site, the C$_{60}$ molecule was initially placed at three different locations (I, II, III). The other Aβ-fullerene/fullerenol systems were constructed similarly, and were immersed in SPC [50] water. Counterions Na$^+$ and Cl$^-$ were added to neutralize the system and provide an additional 0.1 M salt concentration. Systems of isolated Aβ_{42}-trimer and Aβ_{40}-trimer in water were run as control groups.

3.2. Details of MD Simulations

Atomistic MD simulations were performed in isothermal−isobaric (NPT) ensemble using GROMACS-4.5.3 software package [51] with GROMOS96 53a6 force field [52], in accordance with previous computational studies of Aβ peptides [31,33,34,49,53,54]. Periodic boundary conditions were applied in all three directions. The temperature and pressure of the systems were coupled using the Nose−Hoover algorithm [55,56] (310 K, τ_T = 0.2 ps) and Parinello–Rahman algorithm [57,58] (1 bar, τ_P = 1.0 ps), respectively. The simulation time step was 2 fs with all bonds constrained using the LINCS algorithm [59]. The electrostatic interactions were treated with the particle mesh Ewald (PME) method [60] with a cutoff of 1.0 nm, and the van der Waals interactions were calculated using a cutoff of 1.4 nm. For A$\beta_{40/42}$-trimer-C$_{60}$ and A$\beta_{40/42}$-trimer-C$_{60}$(OH)$_6$ systems, six independent copies of each system were carried out, each lasting 50 ns; for A$\beta_{40/42}$-trimer-C$_{60}$(OH)$_{12}$ systems, six independent 100-ns MD runs were carried out; for isolated A$\beta_{40/42}$-trimer systems, two independent 200-ns MD runs were carried out.

3.3. Analysis Methods

Trajectory analysis was performed using the GROMACS-4.5.3 package toolkits and in-house developed codes. The secondary structure was calculated using the DSSP program [61]. Here, an atomic contact is defined when two non-hydrogen atoms come within 0.54 nm. The H-bond is determined using geometrical criteria: the distance between donor D and acceptor A is less than 0.35 nm and the D-H-A angle is larger than 150°. The π-stacking structure is defined when the centroid of residue aromatic ring is within 0.45 nm from the spherical carbon surface of fullerene/fullerenol [62]. The binding energy between a ligand and a receptor was estimated by means of (MM/PBSA) [63,64]: $\Delta G_{bind} = \Delta E_{MM} + \Delta G_{solv} - T\Delta S$, $\Delta E_{MM} = \Delta E_{vdW} + \Delta E_{elec}$, $\Delta G_{solv} = \Delta G_{polar} + \Delta G_{nonpolar}$, $\Delta G_{nonpolar} = \gamma \cdot \text{SASA} + b$. Here, E_{MM} is the gas-phase energy, consisting of electrostatic (ΔE_{elec}) and van der Waals (ΔE_{vdw}) terms; ΔG_{solv} is the sum of polar solvation energy ΔG_{polar} and nonpolar solvation component $\Delta G_{nonpolar}$; ΔG_{polar} is estimated by solving the Poisson−Boltzmann equation; $\Delta G_{nonpolar}$ is estimated by solvent accessible surface area (SASA). A water probe radius of 0.14 nm was used to calculate SASA, and γ (surface tension of the solvent) and b (fitting parameter) were set to 0.542 kcal/mol/nm^2 and 0.92 kcal/mol, respectively. As the binding free energy (ΔG_{bind}) reported here is the relative binding free energy, the contribution of conformational entropy of peptides was ignored in accordance with a number of previous computational studies [33,34,65,66].

4. Conclusions

We investigated the dynamics, sites and interactions of the $C_{60}/C_{60}(OH)_6/C_{60}(OH)_{12}$ nanoparticle binding to $A\beta_{42/40}$ protofibrillar trimer by performing extensive atomistic MD simulations. To our knowledge, this is the first atomistic explicit-solvent simulation study to investigate the binding behavior of fullerenols to $A\beta_{42/40}$ protofibril. Our simulations demonstrate that the higher hydroxylation level of C_{60} leads to slower binding dynamics and weaker binding strength. When binding to $A\beta_{42}$-trimer, C_{60} preferentially interacts with C-terminal residues 31–41 and 2AEF4; $C_{60}(OH)_6$ prefers to bind to C-terminal residues 31–41 and 9GYE11; $C_{60}(OH)_{12}$ favors to bind to *N*-terminal residues 4–14. In addition, the $C_{60}(OH)_6$ molecule has higher affinity to bind to elongation surfaces than C_{60} and $C_{60}(OH)_{12}$. The binding of these nanoparticles has a slight influence on the secondary structure and structural stability of $A\beta_{42}$-trimer during the simulation time. The hydrophobic interaction plays a critical role in the interplay between $A\beta_{42}$ and all three nanoparticles; π-stacking interaction gets weakened as C_{60} carries more hydroxyls. The situations are quite similar when the $C_{60}/C_{60}(OH)_6/C_{60}(OH)_{12}$ nanoparticle binds to $A\beta_{40}$ protofibrillar trimer. Overall, the proper binding strength and high affinity to form hydrogen bonds with protein backbones make the water-soluble $C_{60}(OH)_6$ molecule an efficient inhibitor. This study provides a detailed picture of fullerene/fullerenols binding to $A\beta$ protofibril and expands the understanding of the underlying inhibitory mechanism, which is helpful to the design of novel agents with anti-amyloid properties.

Author Contributions: Conceptualization, P.C. and Z.Q.; methodology, Y.Z. and Z.Q.; software, Y.Z. and Q.Z.; validation, P.C. and Y.L.; formal analysis, Z.L. and Y.Z.; investigation, Q.Z. and Y.L.; resources, Q.Z.; data curation, Z.L. and Y.Z.; writing—original draft preparation, Z.L.; writing—review and editing, Z.Q.

Conflicts of Interest: The authors declare no conflict of interest.

References

1. Jucker, M.; Walker, L.C. Self-propagation of pathogenic protein aggregates in neurodegenerative diseases. *Nature* **2013**, *501*, 45–51. [CrossRef]
2. Knowles, T.P.J.; Vendruscolo, M.; Dobson, C.M. The amyloid state and its association with protein misfolding diseases. *Nat. Rev. Mol. Cell Biol.* **2014**, *15*, 384–396. [CrossRef]
3. Riek, R.; Eisenberg, D.S. The activities of amyloids from a structural perspective. *Nature* **2016**, *539*, 227–235. [CrossRef]
4. Lu, J.X.; Qiang, W.; Yau, W.M.; Schwieters, C.D.; Meredith, S.C.; Tycko, R. Molecular structure of beta-amyloid fibrils in Alzheimer's disease brain tissue. *Cell* **2013**, *154*, 1257–1268. [CrossRef] [PubMed]
5. Gremer, L.; Schölzel, D.; Schenk, C.; Reinartz, E.; Labahn, J.; Ravelli, R.B.G.; Tusche, M.; Lopez-Iglesias, C.; Hoyer, W.; Heise, H.; et al. Fibril structure of amyloid-β(1–42) by cryo–electron microscopy. *Science* **2017**, *358*, 116–119. [CrossRef]
6. Sun, Y.; Wang, B.; Ge, X.; Ding, F. Distinct oligomerization and fibrillization dynamics of amyloid core sequences of amyloid-beta and islet amyloid polypeptide. *Phys. Chem. Chem. Phys.* **2017**, *19*, 28414–28423. [CrossRef]
7. Michaels, T.C.T.; Šarić, A.; Habchi, J.; Chia, S.; Meisl, G.; Vendruscolo, M.; Dobson, C.M.; Knowles, T.P.J. Chemical kinetics for bridging molecular mechanisms and macroscopic measurements of amyloid fibril formation. *Annu. Rev. Phys. Chem.* **2018**, *69*, 273–298. [CrossRef] [PubMed]
8. Kayed, R.; Head, E.; Thompson, J.L.; McIntire, T.M.; Milton, S.C.; Cotman, C.W.; Glabe, C.G. Common structure of soluble amyloid oligomers implies common mechanism of pathogenesis. *Science* **2003**, *300*, 486–489. [CrossRef]
9. Haass, C.; Selkoe, D.J. Soluble protein oligomers in neurodegeneration: Lessons from the Alzheimer's amyloid β-peptide. *Nat. Rev. Mol. Cell Biol.* **2007**, *8*, 101–112. [CrossRef] [PubMed]
10. Straub, J.E.; Thirumalai, D. Toward a molecular theory of early and late events in monomer to amyloid fibril formation. *Annu. Rev. Phys. Chem.* **2011**, *62*, 437–463. [CrossRef]
11. Nguyen, P.; Derreumaux, P. Understanding amyloid fibril nucleation and Aβ oligomer/drug interactions from computer simulations. *Acc. Chem. Res.* **2014**, *47*, 603–611. [CrossRef] [PubMed]

12. Zhang, M.; Mao, X.; Yu, Y.; Wang, C.-X.; Yang, Y.-L.; Wang, C. Nanomaterials for reducing amyloid cytotoxicity. *Adv. Mater.* **2013**, *25*, 3780–3801. [CrossRef]

13. Radic, S.; Davis, T.P.; Ke, P.C.; Ding, F. Contrasting effects of nanoparticle-protein attraction on amyloid aggregation. *RSC Adv.* **2015**, *5*, 105498. [CrossRef]

14. Wang, B.; Pilkington, E.H.; Sun, Y.; Davis, T.P.; Ke, P.C.; Ding, F. Modulating protein amyloid aggregation with nanomaterials. *Environ. Sci. Nano* **2017**, *4*, 1772–1783. [CrossRef]

15. Young, L.M.; Saunders, J.C.; Mahood, R.A.; Revill, C.H.; Foster, R.J.; Tu, L.-H.; Raleigh, D.P.; Radford, S.E.; Ashcroft, A.E. Screening and classifying small-molecule inhibitors of amyloid formation using ion mobility spectrometry–mass spectrometry. *Nat. Chem.* **2014**, *7*, 73–81. [CrossRef]

16. Saunders, J.C.; Young, L.M.; Mahood, R.A.; Jackson, M.P.; Revill, C.H.; Foster, R.J.; Smith, D.A.; Ashcroft, A.E.; Brockwell, D.J.; Radford, S.E. An in vivo platform for identifying inhibitors of protein aggregation. *Nat. Chem. Biol.* **2016**, *12*, 94–101. [CrossRef]

17. Chen, Z.J.; Krause, G.; Reif, B. Structure and orientation of peptide inhibitors bound to β-amyloid fibrils. *J. Mol. Biol.* **2005**, *354*, 760–776. [CrossRef] [PubMed]

18. Takahashi, T.; Mihara, H. Peptide and protein mimetics inhibiting amyloid β-peptide aggregation. *Acc. Chem. Res.* **2008**, *41*, 1309–1318. [CrossRef] [PubMed]

19. Sevigny, J.; Chiao, P.; Bussière, T.; Weinreb, P.H.; Williams, L.; Maier, M.; Dunstan, R.; Salloway, S.; Chen, T.; Ling, Y.; et al. The antibody aducanumab reduces Aβ plaques in Alzheimer's disease. *Nature* **2016**, *537*, 50–56. [CrossRef]

20. Liao, Q.; Owen, M.C.; Bali, S.; Barz, B.; Strodel, B. Aβ under stress: The effects of acidosis, Cu2+-binding, and oxidation on amyloid β-peptide dimers. *Chem. Commun.* **2018**, *54*, 7766–7769. [CrossRef]

21. Xiao, L.; Aoshima, H.; Saitoh, Y.; Miwa, N. Highly hydroxylated fullerene localizes at the cytoskeleton and inhibits oxidative stress in adipocytes and a subcutaneous adipose-tissue equivalent. *Free Radical Biol. Med.* **2011**, *51*, 1376–1389. [CrossRef]

22. Grebowski, J.; Kazmierska, P.; Krokosz, A. Fullerenols as a new therapeutic approach in nanomedicine. *BioMed Res. Int.* **2013**, *2013*, 9. [CrossRef]

23. Bosi, S.; Da Ros, T.; Spalluto, G.; Prato, M. Fullerene derivatives: An attractive tool for biological applications. *Eur. J. Med. Chem.* **2003**, *38*, 913–923. [CrossRef] [PubMed]

24. Dugan, L.L.; Turetsky, D.M.; Du, C.; Lobner, D.; Wheeler, M.; Almli, C.R.; Shen, C.K.F.; Luh, T.Y.; Choi, D.W.; Lin, T.S. Carboxyfullerenes as neuroprotective agents. *Proc. Natl. Acad. Sci. USA* **1997**, *94*, 9434–9439. [CrossRef] [PubMed]

25. Kim, J.E.; Lee, M. Fullerene inhibits β-amyloid peptide aggregation. *Biochem. Biophys. Res. Commun.* **2003**, *303*, 576–579. [CrossRef]

26. Podolski, I.Y.; Podlubnaya, Z.A.; Kosenko, E.A.; Mugantseva, E.A.; Makarova, E.G.; Marsagishvili, L.G.; Shpagina, M.D.; Kaminsky, Y.G.; Andrievsky, G.V.; Klochkov, V.K. Effects of hydrated forms of C60 fullerene on amyloid 1-peptide fibrillization in vitro and performance of the cognitive task. *J. Nanosci. Nanotechnol.* **2007**, *7*, 1479–1485. [CrossRef]

27. Ye, S.; Zhou, T.; Pan, D.; Lai, Y.; Yang, P.; Chen, M.; Wang, Y.; Hou, Z.; Ren, L.; Jiang, Y. Fullerene C60 derivatives attenuated microglia-mediated prion peptide neurotoxicity. *J. Biomed. Nanotechnol.* **2016**, *12*, 1820–1833. [CrossRef] [PubMed]

28. Hsieh, F.-Y.; Zhilenkov, A.V.; Voronov, I.I.; Khakina, E.A.; Mischenko, D.V.; Troshin, P.A.; Hsu, S.-h. Water-soluble fullerene derivatives as brain medicine: Surface chemistry determines if they are neuroprotective and antitumor. *ACS Appl. Mat. Interfaces* **2017**, *9*, 11482–11492. [CrossRef]

29. Huy, P.D.Q.; Li, M.S. Binding of fullerenes to amyloid beta fibrils: Size matters. *Phys. Chem. Chem. Phys.* **2014**, *16*, 20030–20040. [CrossRef]

30. Bednarikova, Z.; Huy, P.D.Q.; Mocanu, M.-M.; Fedunova, D.; Li, M.S.; Gazova, Z. Fullerenol C60(OH)16 prevents amyloid fibrillization of Aβ40 – in vitro and in silico approach. *Phys. Chem. Chem. Phys.* **2016**, *18*, 18855–18867. [CrossRef]

31. Zhou, X.Y.; Xi, W.H.; Luo, Y.; Cao, S.Q.; Wei, G.H. Interactions of a water-soluble fullerene derivative with amyloid-beta protofibrils: Dynamics, binding mechanism, and the resulting salt-bridge disruption. *J. Phys. Chem. B* **2014**, *118*, 6733–6741. [CrossRef] [PubMed]

32. Radic, S.; Nedumpully-Govindan, P.; Chen, R.; Salonen, E.; Brown, J.M.; Ke, P.C.; Ding, F. Effect of fullerenol surface chemistry on nanoparticle binding-induced protein misfolding. *Nanoscale* **2014**, *6*, 8340–8349. [CrossRef] [PubMed]

33. Xie, L.; Luo, Y.; Lin, D.; Xi, W.; Yang, X.; Wei, G. The molecular mechanism of fullerene-inhibited aggregation of Alzheimer's β-amyloid peptide fragment. *Nanoscale* **2014**, *6*, 9752–9762. [CrossRef]

34. Sun, Y.; Qian, Z.; Wei, G. The inhibitory mechanism of a fullerene derivative against amyloid-β peptide aggregation: An atomistic simulation study. *Phys. Chem. Chem. Phys.* **2016**, *18*, 12582–12591. [CrossRef] [PubMed]

35. Zhao, J.; Wang, Q.; Liang, G.; Zheng, J. Molecular dynamics simulations of low-ordered Alzheimer β-amyloid oligomers from dimer to hexamer on self-assembled monolayers. *Langmuir* **2011**, *27*, 14876–14887. [CrossRef] [PubMed]

36. Sun, Y.; Xi, W.; Wei, G. Atomic-level study of the effects of O4 molecules on the structural properties of protofibrillar Abeta trimer: Beta-sheet stabilization, salt bridge protection, and binding mechanism. *J. Phys. Chem. B* **2015**, *119*, 2786–2794. [CrossRef] [PubMed]

37. Ngo, S.T.; Li, M.S. Curcumin binds to Aβ1–40 peptides and fibrils stronger than ibuprofen and naproxen. *J. Phys. Chem. B* **2012**, *116*, 10165–10175. [CrossRef] [PubMed]

38. Thai, N.Q.; Nguyen, H.L.; Linh, H.Q.; Li, M.S. Protocol for fast screening of multi-target drug candidates: Application to Alzheimer's disease. *J. Mol. Graphics Modell.* **2017**, *77*, 121–129. [CrossRef]

39. Andujar, S.A.; Lugli, F.; Hofinger, S.; Enriz, R.D.; Zerbetto, F. Amyloid-beta fibril disruption by C60-molecular guidance for rational drug design. *Phys. Chem. Chem. Phys.* **2012**, *14*, 8599–8607. [CrossRef] [PubMed]

40. Benyamini, H.; Shulman-Peleg, A.; Wolfson, H.J.; Belgorodsky, B.; Fadeev, L.; Gozin, M. Interaction of C60-fullerene and carboxyfullerene with proteins: Docking and binding site alignment. *Bioconjugate Chem.* **2006**, *17*, 378–386. [CrossRef]

41. Do, T.D.; LaPointe, N.E.; Nelson, R.; Krotee, P.; Hayden, E.Y.; Ulrich, B.; Quan, S.; Feinstein, S.C.; Teplow, D.B.; Eisenberg, D.; et al. Amyloid β-protein C-terminal fragments: Formation of cylindrins and β-barrels. *J. Am. Chem. Soc.* **2016**, *138*, 549–557. [CrossRef]

42. Truex, N.L.; Wang, Y.; Nowick, J.S. Assembly of peptides derived from β-sheet regions of β-amyloid. *J. Am. Chem. Soc.* **2016**, *138*, 13882–13890. [CrossRef]

43. Qian, Z.; Zhang, Q.; Liu, Y.; Chen, P. Assemblies of amyloid-β30–36 hexamer and its G33V/L34T mutants by replica-exchange molecular dynamics simulation. *PLoS ONE* **2017**, *12*, e0188794. [CrossRef]

44. Kar, R.K.; Brender, J.R.; Ghosh, A.; Bhunia, A. Nonproductive binding modes as a prominent feature of Aβ40 fiber elongation: Insights from molecular dynamics simulation. *J. Chem. Inf. Model.* **2018**, *58*, 1576–1586. [CrossRef]

45. Brender, J.R.; Ghosh, A.; Kotler, S.A.; Krishnamoorthy, J.; Bera, S.; Morris, V.; Sil, T.B.; Garai, K.; Reif, B.; Bhunia, A.; et al. Probing transient non-native states in amyloid beta fiber elongation by NMR. *Chem. Commun.* **2019**, *55*, 4483–4486. [CrossRef] [PubMed]

46. Ferkinghoff-Borg, J.; Fonslet, J.; Andersen, C.B.; Krishna, S.; Pigolotti, S.; Yagi, H.; Goto, Y.; Otzen, D.; Jensen, M.H. Stop-and-go kinetics in amyloid fibrillation. *Phys. Rev. E* **2010**, *82*, 010901. [CrossRef] [PubMed]

47. Melchor, M.-H.; Susana, F.-G.; Francisco, G.-S.; Hiram, I.B.; Norma, R.-F.; Jorge, A.L.-R.; Perla, Y.L.-C.; Gustavo, B.-I. Fullerenemalonates inhibit amyloid beta aggregation, in vitro and in silico evaluation. *RSC Adv.* **2018**, *8*, 39667–39677. [CrossRef]

48. Gazit, E. A possible role for π-stacking in the self-assembly of amyloid fibrils. *FASEB J.* **2002**, *16*, 77–83. [CrossRef]

49. Xie, L.G.; Lin, D.D.; Luo, Y.; Li, H.Y.; Yang, X.J.; Wei, G.H. Effects of Hydroxylated Carbon Nanotubes on the Aggregation of A beta(16-22) Peptides: A Combined Simulation and Experimental Study. *Biophys. J.* **2014**, *107*, 1930–1938. [CrossRef]

50. Berendsen, H.; Postma, J.; Van Gunsteren, W.; Hermans, J. Interaction models for water in relation to protein hydration. *Intermol. Forces* **1981**, *11*, 331–342.

51. Pronk, S.; Pall, S.; Schulz, R.; Larsson, P.; Bjelkmar, P.; Apostolov, R.; Shirts, M.R.; Smith, J.C.; Kasson, P.M.; van der Spoel, D.; et al. GROMACS 4.5: A high-throughput and highly parallel open source molecular simulation toolkit. *Bioinformatics* **2013**, *29*, 845–854. [CrossRef]

52. Oostenbrink, C.; Villa, A.; Mark, A.E.; van Gunsteren, W.F. A biomolecular force field based on the free enthalpy of hydration and solvation: The GROMOS force-field parameter sets 53A5 and 53A6. *J. Comput. Chem.* **2004**, *25*, 1656–1676. [CrossRef]

53. Nguyen, P.H.; Li, M.S.; Stock, G.; Straub, J.E.; Thirumalai, D. Monomer adds to preformed structured oligomers of Aβ-peptides by a two-stage dock-lock mechanism. *Proc. Natl. Acad. Sci. USA* **2007**, *104*, 111–116. [CrossRef]

54. Krone, M.G.; Hua, L.; Soto, P.; Zhou, R.; Berne, B.J.; Shea, J.E. Role of water in mediating the assembly of Alzheimer amyloid-β Aβ16-22 protofilaments. *J. Am. Chem. Soc.* **2008**, *130*, 11066–11072. [CrossRef]

55. Nosé, S. A molecular dynamics method for simulations in the canonical ensemble. *Mol. Phys.* **1984**, *52*, 255–268. [CrossRef]

56. Hoover, W.G. Canonical dynamics: Equilibrium phase-space distributions. *Phys. Rev. A* **1985**, *31*, 1695–1697. [CrossRef]

57. Parrinello, M.; Rahman, A. Polymorphic transitions in single crystals: A new molecular dynamics method. *J. Appl. Phys.* **1981**, *52*, 7182–7190. [CrossRef]

58. Nosé, S.; Klein, M.L. Constant pressure molecular dynamics for molecular systems. *Mol. Phys.* **1983**, *50*, 1055–1076. [CrossRef]

59. Hess, B.; Bekker, H.; Berendsen, H.J.C.; Fraaije, J.G.E.M. LINCS: A linear constraint solver for molecular simulations. *J. Comput. Chem.* **1997**, *18*, 1463–1472. [CrossRef]

60. Darden, T.; York, D.; Pedersen, L. Particle mesh Ewald - an N.Log(N) method for Ewald sums in large systems. *J. Chem. Phys.* **1993**, *98*, 10089–10092. [CrossRef]

61. Kabsch, W.; Sander, C. Dictionary of protein secondary structure - pattern-recognition of hydrogen-bonded and geometrical features. *Biopolymers* **1983**, *22*, 2577–2637. [CrossRef]

62. Xu, Z.; Lei, X.; Tu, Y.; Tan, Z.-J.; Song, B.; Fang, H. Dynamic cooperation of hydrogen binding and π stacking in ssDNA adsorption on graphene oxide. *Chem.-Eur. J.* **2017**, *23*, 13100–13104. [CrossRef] [PubMed]

63. Luo, R.; David, L.; Gilson, M.K. Accelerated Poisson–Boltzmann calculations for static and dynamic systems. *J. Comput. Chem.* **2002**, *23*, 1244–1253. [CrossRef]

64. Kumari, R.; Kumar, R.; Lynn, A. g_mmpbsa—A GROMACS tool for high-throughput MM-PBSA calculations. *J. Chem. Inf. Model.* **2014**, *54*, 1951–1962. [CrossRef] [PubMed]

65. Berhanu, W.M.; Hansmann, U.H.E. The stability of cylindrin β-barrel amyloid oligomer models—A molecular dynamics study. *Proteins* **2013**, *81*, 1542–1555. [CrossRef] [PubMed]

66. Zou, Y.; Qian, Z.; Chen, Y.; Qian, H.; Wei, G.; Zhang, Q. Norepinephrine inhibits Alzheimer's amyloid-β peptide aggregation and destabilizes amyloid-β protofibrils: A molecular dynamics simulation study. *ACS Chem. Neurosci.* **2019**, *10*, 1585–1594. [CrossRef]